Paper AAS 06-xxx

Jupiter Icy Moons Orbiter Interplanetary Injection Period Analysis

Theresa D. Kowalkowski, Julie A. Kangas, and Daniel W. Parcher
Jet Propulsion Laboratory
California Institute of Technology
Pasadena, California

16th AAS/AIAA Space Flight Mechanics Conference

Tampa, Florida **January 22-26, 2006**

AAS Publications Office, P.O. Box 28130, San Diego, CA 92198

JUPITER ICY MOONS ORBITER INTERPLANETARY INJECTION PERIOD ANALYSIS

Theresa D. Kowalkowski,[*] Julie A. Kangas,[†] and Daniel W. Parcher[‡]

This paper investigates the sensitivity of the planned Jupiter Icy Moons Orbiter mission to variations in interplanetary injection date, magnitude, and direction, starting in a low-Earth assembly orbit. These results are used to determine the frequency and number of injection opportunities from a precessing assembly obit. It is shown that the use of a low-thrust propulsion system with a nuclear-electric power source would allow the interplanetary trajectory performance to be relatively insensitive to variations in injection conditions. This result yields many injection opportunities due to the long injection period and consecutive orbits with favorable geometry.

INTRODUCTION

The proposed Jupiter Icy Moons Orbiter (JIMO) mission would employ a nuclear-electric propulsion (NEP) system to both rendezvous with Jupiter and explore three of its "icy" satellites: Callisto, Ganymede, and Europa. It is well-documented that highly-efficient electric-propulsion systems allow interplanetary missions to deliver more mass and/or reduce the flight times to their targets.[1-12] The NEP system is an enabling technology for the planned JIMO mission because of the mission's high ΔV requirements.

The JIMO architecture considered here calls for multiple launches into a low-Earth assembly orbit. After assembly completion, the spacecraft would inject to a positive Earth-departure energy (C_3). In this paper, we investigate the mass-performance impact of varying the interplanetary injection date on four different trajectories: 6-year direct, 7.5-year direct, 6-year Earth gravity assist, and the JIMO Reference Trajectory representation (a 5.5-yr direct case). Next, we explore the effects of variations in the injection burn direction and magnitude. Finally, these results are used to ascertain the frequency and number of injection opportunities from the precessing assembly orbit.

DEFINITIONS AND MODELS

The term *injection* refers to the departure from the assembly orbit onto an interplanetary trajectory. The *injection period* is defined as the number of consecutive days during which the spacecraft can inject

[*] Member of Engineering Staff; Guidance, Navigation, and Control Section; Jet Propulsion Laboratory, California Institute of Technology, Mail Stop 301-150, 4800 Oak Grove Drive, Pasadena, California, 91109-8099.
E-mail: Theresa.D.Kowalkowski@jpl.nasa.gov. Phone: (818) 354-4699. Fax: (818) 393-7116.

[†] Senior Member of Engineering Staff; Guidance, Navigation, and Control Section; Jet Propulsion Laboratory, California Institute of Technology, Mail Stop 301-150, 4800 Oak Grove Drive, Pasadena, California, 91109-8099.
E-mail: Julie.A.Kangas@jpl.nasa.gov. Phone: (818) 354-8285. Fax: (818) 393-7413.

[‡] Member of Engineering Staff; Guidance, Navigation, and Control Section; Jet Propulsion Laboratory, California Institute of Technology, Mail Stop 230-205, 4800 Oak Grove Drive, Pasadena, California, 91109-8099.
E-mail: Daniel.W.Parcher@jpl.nasa.gov. Phone: (818) 393-0457. Fax: (818) 393-4215.

and still deliver sufficient mass to Jupiter. This is analogous to a conventional launch period, but the proposed JIMO architecture requires the distinction between launch and injection because the spacecraft could spend a substantial amount of time in the assembly orbit (weeks or more).

We define the *injection vector sensitivity* to be the effects of deviations in the magnitude and direction of the injection burn from their optimized values. Although we do not model the finite burn, we introduce dispersions in the optimal values of the Earth departure V_∞ (hyperbolic excess velocity) vector.

Finally, an *injection opportunity* is defined as each time the spacecraft and the assembly orbit are aligned in the proper injection direction, within a specified tolerance. Because the node of the assembly orbit precesses around the Earth, not every orbit will have an injection opportunity.

The spacecraft is assumed to have a 180 kW nuclear power supply with a 7000 second specific impulse (Isp) and an efficiency of 70% (corresponding to 3.67 N of thrust and a 5.35×10^{-5} kg/s mass flow rate). The spacecraft is constrained to coast for 60 days after injection for reactor commissioning. When the initial mass and departure energy are optimized, the injection vehicle curve shown in Figure 1 is used.

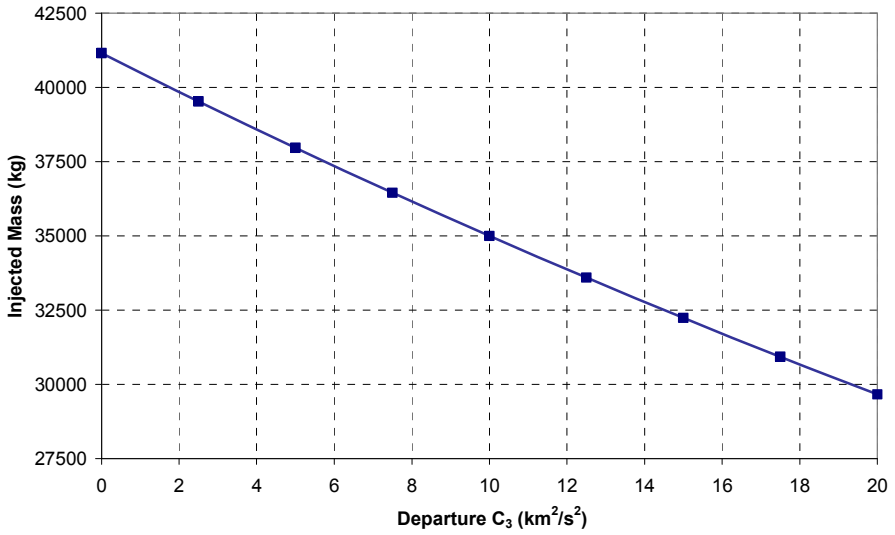

Figure 1 – Injection vehicle performance curve

The majority of the trajectory optimization studies in this paper were performed with the Mission Analysis Low-Thrust Optimization program (MALTO). MALTO is a patched-conic propagator that models low-thrust arcs as a series of small, impulsive maneuvers and maximizes the final mass of the spacecraft.[13] The only forces modeled are the sun's gravity and the spacecraft thrust. No other bodies have mass, and solar radiation pressure is not included. For rendezvous with Jupiter, the spacecraft matches Jupiter's position and velocity, but the planet itself has no gravitational pull. Earth departure is from a massless Earth, and gravity-assist maneuvers are modeled as instantaneous rotations of the V_∞ vector.

A few select analyses were carried out using Mystic, a low-thrust trajectory optimization tool that also maximizes the final mass of the spacecraft.[14] Mystic fully integrates trajectories with low-thrust arcs modeled as a series of continuous-thrust segments. The thrust has a constant magnitude and direction over a given segment. In these studies, the forces modeled are the Sun's gravity, Mars's gravity, Jupiter's gravity, (with no oblateness for any of the planets) and the spacecraft thrust. Earth's gravity was not modeled; the trajectory starts at the center of the massless Earth (as in the MALTO analyses). No solar radiation

pressure was modeled, either. Mystic targeted a final distance from Jupiter of less than 2,000,000 km at less than 0 km^2/s^2 two-body energy with respect to Jupiter.

Although it is a lower-fidelity tool than Mystic, MALTO's speed and ease of use makes it particularly well-suited to performing parametric studies. We will show that the results from MALTO are somewhat conservative relative to Mystic but the MALTO findings are an excellent indicator of trends and overall behavior.

For the investigation of injection opportunities, a representative assembly orbit of 400 km altitude and inclination of 28.5º was propagated with a 50x50 Earth gravity field. The initial right ascension of the ascending node (RAAN) was chosen such that the first injection opportunity would be available soon after the open of the injection period.

TRAJECTORY CASES

Although the planned JIMO mission assumed a baseline trajectory, called the Reference Trajectory,[15] we present results from three additional trajectory types. Many of the analyses on these other trajectories preceded and influenced the selection of the Reference Trajectory type. In addition, the results presented here are documented for the sake of potential future mission design efforts.

Three of the four representative trajectories in this paper use the injection vehicle performance curve given in Figure 1. The fourth trajectory assumes a bounded departure C_3 magnitude and mass, discussed below. All four trajectories were optimized assuming a fixed flight time, but the software optimized the injection and arrival dates, the injection vector, and the corresponding initial mass. Each trajectory is assigned a case number for the sake of discussion, but no priority is implied by the numbering scheme.

The trajectory designated Case 1 is a 6-year direct case to Jupiter with a little more than 1.5 heliocentric revolutions (see Table 1). Case 1 has only one optimal coast arc and the rest of the time is spent thrusting (Figure 2). Case 2 is also a direct trajectory but with a 7.5-year flight time and just under 2.5 solar revolutions. This case has two optimal coasting arcs: the first is after about 1.5 revolutions, and the second is prior to the Jupiter-rendezvous thrust period.

Table 1 – Summary of trajectory characteristics

Case	Software	Traj. Type	Revs.	Flight Time (yrs)	Optimized Injection Date	Optimized Arrival Date	Injection C_3 (km^2/s^2)	Injection Mass (kg)	Arrival Mass (kg)
1	MALTO	Direct	1.5	6	10/20/2015	12/20/2021	5.06	37,925	30,451
2	MALTO	Direct	2.5	7.5	12/21/2014	06/21/2022	0.33	40,932	32,471
3	MALTO	EEJ	2.5	6	02/19/2015	02/19/2021	2.73	39,385	32,945
4a	Mystic	Direct	1.5	5.5	12/09/2015	06/10/2021	10.0	36,000	30,886
4b	MALTO	Direct	1.5	5.7	12/26/2015	09/19/2021	10.0	36,000	29,957

The Case 3 trajectory is the final trajectory that uses the injection vehicle performance curve. This trajectory has a 6-year time of flight, like Case 1, but it includes an Earth gravity assist, making it an Earth-Earth-Jupiter (EEJ) trajectory. The trajectory is referred to as a 3:2i trajectory[11] because there are approximately three Earth revolutions during the nearly two spacecraft revolutions on the Earth-Earth transfer, and the Earth flyby occurs when the spacecraft is moving inbound toward the Sun, as shown in Figure 2. The spacecraft was constrained to an Earth flyby radius of at least 7000 km. After the Earth gravity assist, there is roughly half a revolution on the Earth-Jupiter leg.

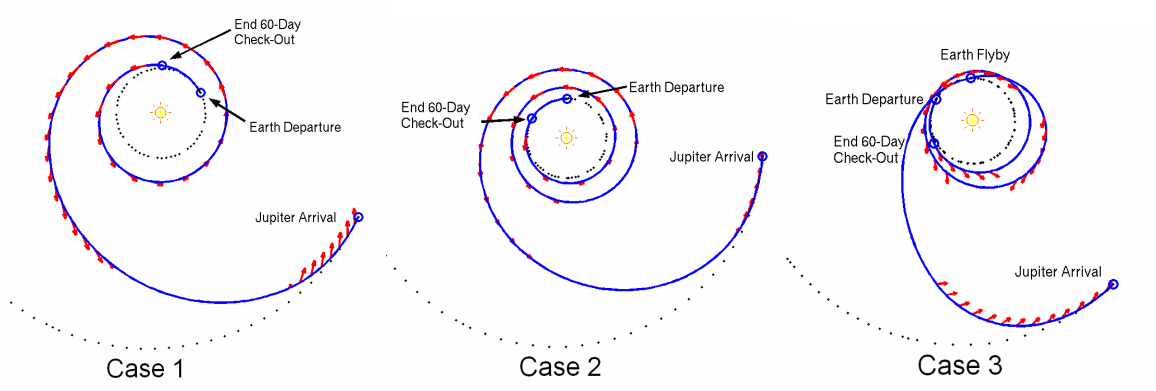

Figure 2 – Trajectory Cases 1-3. Case 1 is a 6-year direct trajectory, Case 2 is a 7.5-year direct trajectory, and Case 3 is a 6-year Earth-Earth-Jupiter (EEJ) trajectory.

The last trajectory is Case 4, and it is a representation of the interplanetary portion of the proposed JIMO Reference Trajectory.[15] This trajectory does not use the injection vehicle curve given in Figure 1 but instead has a constrained injection energy and mass. The JIMO architecture assumed for Case 4 has upper stages capable of injecting 36,000 kg to C_3=10 km^2/s^2. Since the planned launch vehicle would only be able to loft a 36,000 kg spacecraft into the assembly orbit, injecting to a lower C_3 could not result in a higher initial mass. The optimization programs described above were free to use a lower energy, but lower injection energies did not yield a greater initial mass.

Case 4 is a direct trajectory and is subdivided into Cases 4a and 4b (see Figure 3). Case 4a was generated using Mystic, the high-fidelity low-thrust optimization tool, and was constrained to a 5.5-year flight time. Case 4b was produced with MALTO and was crafted to resemble the Mystic representation in terms of optimal coast arcs and thrusting periods.

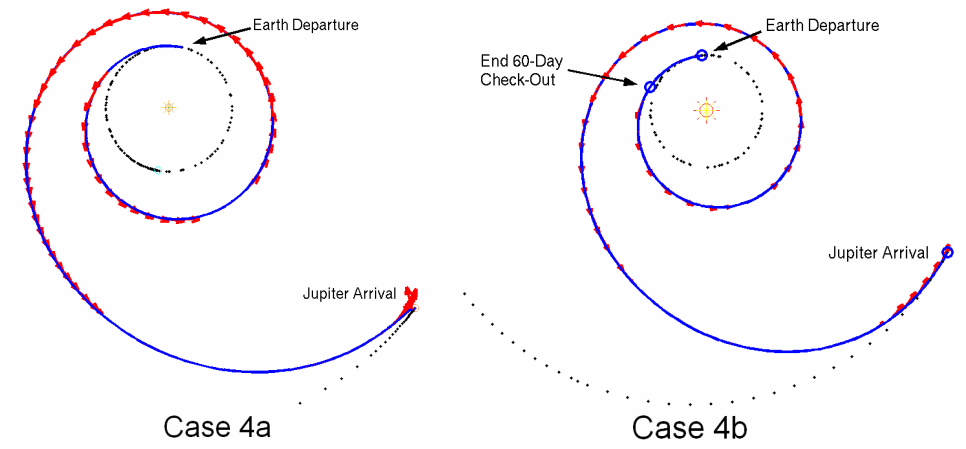

Figure 3 – Mystic (4a) and MALTO (4b) representations of the Reference Trajectory

Case 4b is allowed a longer flight time (5.7 years) and an arrival V_∞ magnitude of 0.5 km/s to accommodate the two major differences between MALTO and Mystic in the Jupiter arrival models and constraints. First, MALTO requires an exact match in position with Jupiter, but a non-zero V_∞ magnitude can be permitted (positive energy). Mystic, on the other hand, allows the spacecraft to be 2,000,000 km from the center of Jupiter at the trajectory's end state, but the two-body energy with respect to Jupiter was re-

quired to be less than or equal to 0 km^2/s^2. Second, Mystic models Jupiter's gravity while MALTO does not.

Hence, Case 4b uses different constraints than Case 4a, but both trajectories exhibit very similar thrust profiles, which was desired to yield comparable sensitivities to injection conditions. While Case 4b's final mass is lower than Mystic's (Table 1), it is shown in a later section that the sensitivity to the injection vector is quite similar for both.

INJECTION PERIOD

Approach

The objective behind a launch period analysis is to determine the sensitivity of the delivered mass to sub-optimal launch dates near the optimal value. This is normally done to account for any issues with equipment, software, weather, or any other circumstances that might occur just prior to launch preventing launch from occurring at the optimal time. The analysis performed here differs from that somewhat since we are examining the performance sensitivity to interplanetary injection from the assembly orbit, rather than launch from the ground. As a result, the injection period must account for a different suite of problems such as delays in on-orbit assembly, delays in component launches, or spacecraft hardware or software problems.

To determine the injection period sensitivity, we examine each of the trajectories listed in the previous section, in addition to examining different mission scenarios and alternate trajectory families. We begin with a discussion of the injection periods for trajectory Cases 1 through 4a. Next, we expand this analysis to include alternative arrival dates and trajectory types in the hopes of increasing the injection window. Since delays to injection may occur after the spacecraft has been launched into the assembly orbit, the spacecraft mass and injection C_3 must remain fixed at the optimized values for the nominal trajectory. While different trajectory types are explored to extend the injection period, the fixed injection mass and C_3 may be sub-optimal for these additional trajectory families.

The injection period performance profile for the different trajectory scenarios was generated by first optimizing the injection and arrival dates of each case for the fixed flight time given in Table 1. In Cases 1-3, the injection C_3 and mass were also optimized. Then, the optimal arrival date, injection C_3, and initial spacecraft mass were held fixed while the injection date was varied parametrically. The optimized arrival date was retained to preserve the tour of the Jovian system, which eliminated the need for a complicated and time-consuming redesign of the moon tour. Finally, the thrust profile was re-optimized at each value of the injection date to deliver the greatest possible mass to Jupiter.

Results

The injection period for trajectory Cases 1-4a is shown in Figure 4 in percent change of delivered mass with respect to the optimal value. Normalizing the delivered mass by the optimal value for each case and plotting the results together provides some insight into the relative sensitivities of the different trajectory types.

Case 1

Trajectory Case 1 is the most sensitive to suboptimal injection dates in terms of delivered mass. However, the performance penalty for injecting prior to the optimal date is less than the penalty for late injection. A 100-day injection period requires only a 1.5% loss in performance with respect to the optimal delivered mass. The fact that Case 1 is the most sensitive to suboptimal injection dates is partly due to the

short flight time. Only Case 4a is shorter, and it benefits from Jupiter's gravitational pull on approach to rendezvous, whereas this case does not. Case 3 has a comparable flight time, but the Earth gravity assist appears to offer reduced sensitivity to the injection date.

As injection is moved past the optimal injection date, Case 1, as with all of the cases here, reaches a point where the delivered mass begins to drop off quite quickly. This "cliff" effect in the performance is caused by the shortening, and eventually the closing, of optimal coast arcs in the trajectory. The result is a fairly inefficient thrust profile that sacrifices a significant amount of propellant to achieve the required arrival date. The performance "cliff" in Case 1 occurs almost immediately as the injection date is delayed from the optimal value. Case 1 has the fewest optimal coast arcs of all the trajectories considered (Figure 2), so it is expected that it would be the most sensitive to sub-optimal injection conditions.

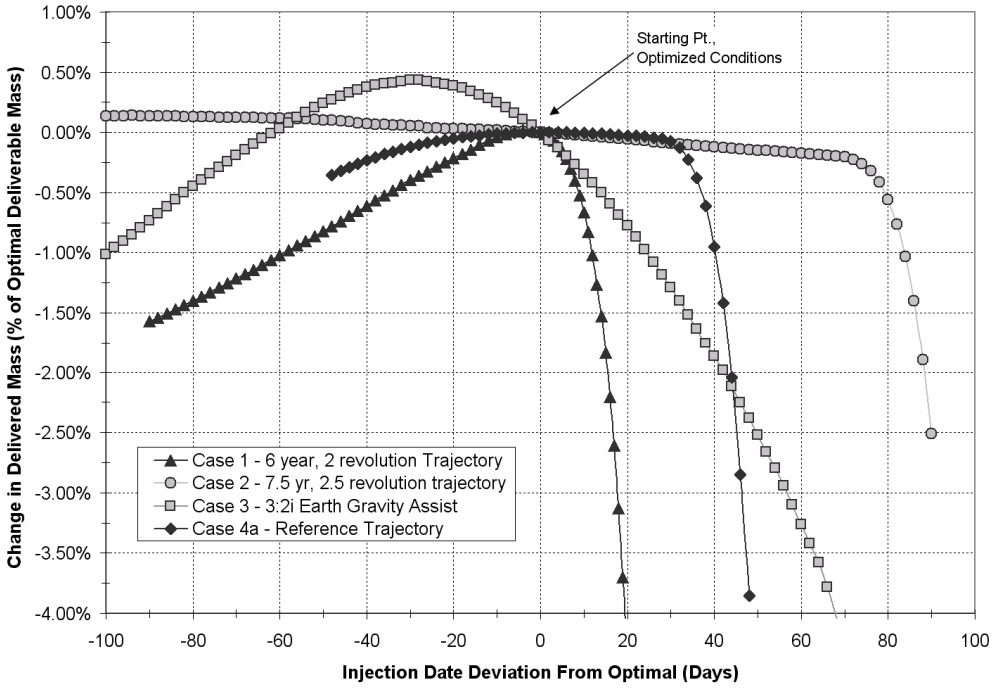

Figure 4 – Interplanetary trajectory performance sensitivity to injection date

Case 2

The performance curve for trajectory Case 2 is also shown in Figure 4. The optimal C_3 at the starting point for this trajectory is the lowest of all of the cases (0.33 km^2/s^2). The low initial C_3 is a result of the longer flight time and additional heliocentric revolution for this Case. Both of these characteristics contribute to a substantially reduced sensitivity to the injection period.

Early injection in this case results in an increase in mass due to increased flight time. Since the C_3 is low, the trajectory benefits more from the increased flight time than it loses from the change in injection geometry. As a result, an injection period for this is indefinite. Consider as an example the case where the injection C_3 is zero. In this case, "injection" simply refers to waiting for the most opportune time to begin thrusting for Earth departure. This means that the spacecraft can be "injected" to a C_3 of zero at any time prior to the optimal date, and as long as thrusting starts at the optimal point, no performance is lost.[§] A similar effect is occurring in Case 2.

[§] The Earth is modeled as a massless body in these trajectory scenarios.

Note that the "cliff" in performance exists for this case much as it did in Case 1. In this case, the sudden drop in performance occurs roughly 70 days after the optimal injection point. This is significantly later than the results for the other trajectories. Again, the low C_3 results in a lack of sensitivity to suboptimal injection geometries, while having additional flight time (1.5 years over trajectory Case 1, for example) means that optimal coast arcs are longer, and don't close until the injection date delay is more significant.

Case 3

Also shown in Figure 4 is the injection period performance for the 3:2i Earth gravity-assist case (trajectory Case 3). For the gravity assist case, injecting less than 30 days early results in an increase in delivered mass due to the corresponding increase in flight time. However, the delivered mass begins to decrease again when injection occurs more than 30 days early. This is due to the change in phase angle between Earth and Jupiter. Once again, we see that injecting after the optimal point causes a sudden, although less severe, drop off in performance. However, this does not occur until injection has been delayed by two months.

When compared to the other 6-year trajectory, Case 1, the Earth gravity-assist case appears to have less sensitivity to variations in injection date. An injection period of 100 days would yield slightly more than 0.5% loss in delivered mass as compared to the 1.5% loss in Case 1.

Case 4a

Finally, the performance vs. injection curve for the JIMO baseline case, trajectory Case 4a, is also shown in Figure 4. The trajectory exhibits low sensitivity to variations in injection date until over a month past the optimal injection date. Injecting early, however, has little performance impact for all of the injection dates investigated here. Allowing the mass at Jupiter capture to reduce by only ~0.35% of the optimal delivered mass results in a generous injection period of over 80 days. As previously stated, the reduced sensitivity of this case versus Case 1 is likely due to the presence of Jupiter's gravity in the trajectory simulation and shortening the final approach thrust arc, which reduces the sensitivity of the trajectory to the changes in flight time and phasing introduced by varying the injection date.

Delays in Arrival Date

Our first attempt to mitigate the performance drop off seen in each of the cases in Figure 4 is to simply delay the Jupiter arrival date in integer numbers of Callisto periods. By restricting the delay to integer numbers of Callisto periods, the impact on the capture at Jupiter is minimized since a Callisto flyby on Jupiter approach has been baselined.[15] The arrival date was allowed to "slip" 1 and then 5 Callisto periods, and the parametric variation of injection date was performed as before, though the C_3 and mass were not reoptimized. This simulates what affect a post-launch, but pre-injection delay to the arrival date might have on performance. The Case 1 injection period performance for both the nominal and delayed arrival dates is shown in Figure 5.

The results of all three scenarios shown in Figure 5 indicate that, as before, significantly less performance is lost by injecting early than is lost by injecting late. At injections 20 days past the optimal injection date all three cases lose roughly 5% deliverable mass with respect to each case's optimal value. Delaying the arrival by 5 Callisto periods (83.45 days) delays the "cliff" in performance by only a few days and does little to extend the injection period.

The delivered masses in the delayed arrival cases are higher than the nominal case due to the increased flight time. By increasing the flight time, coast arcs can be extended slightly in the interplanetary trajectory, thereby increasing the efficiency of the thrust and reducing the propellant consumption. Had the case been completely re-optimized (including injection C_3) the mass delivered to Jupiter for the delayed

arrival case would be even larger. However, the changes to the upper stage propellant loading to achieve these C_3's would be difficult to achieve after launch, so this scenario was not investigated further.

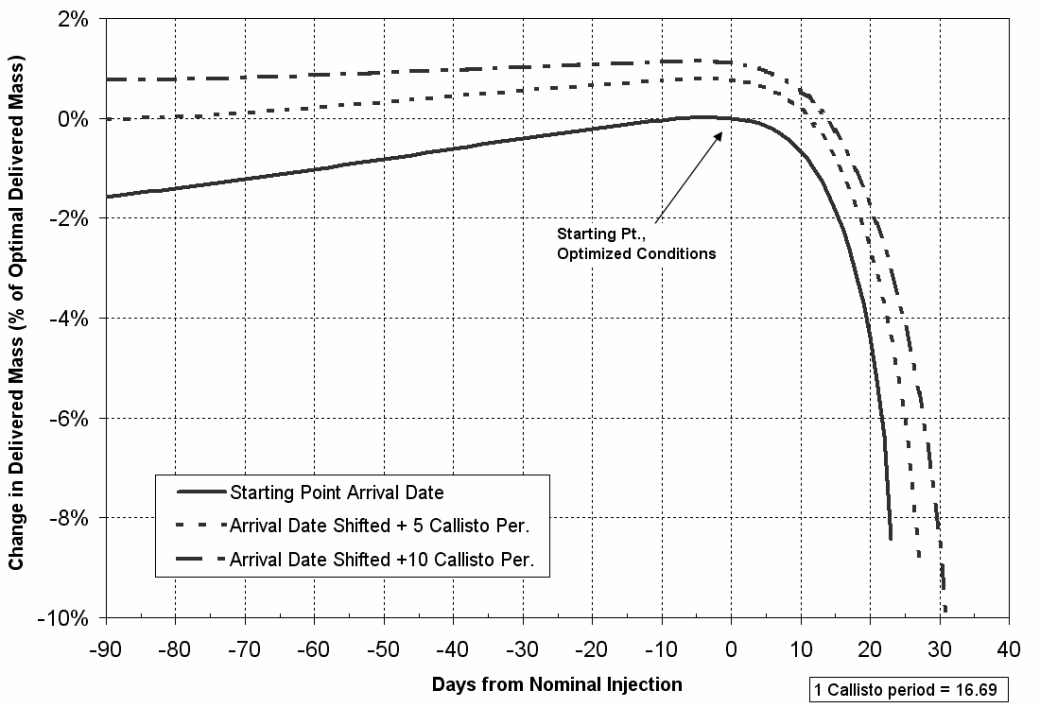

Figure 5 – Direct 6-year (Case 1) trajectory injection period and effect of delayed arrival

Since the delays to the arrival date were unable to extend the injection period past the optimal injection date significantly, we began investigating alternative ways to take advantage of a delay in arrival date.

Alternate Trajectory Types

Figure 6 shows how considering alternative trajectory families can offer extended injection opportunities. Case A in the figure indicates the performance capability of trajectory Case 1 with its nominal arrival date, also shown in Figure 5. Case descriptions for the other scenarios in Figure 6 are listed in Table 2.

Case B is the same trajectory type as Case A but with the arrival date delayed 5 Callisto periods. Case C in Figure 6 illustrates the performance obtained for a trajectory that arrives roughly 7 months after Case A and performs 2.5 revolutions about the sun, one revolution more than Case A. For this case, the injection C_3 and mass are still constrained to the optimal value for Case A. This is done to simulate the need to switch families after the spacecraft has been launched to the assembly orbit but before it has been injected onto its interplanetary path. This constraint on C_3 and injected mass is the reason that Case C underperforms Cases A and B for injection dates less than +25 days from the nominal.

Finally, we verified that it is indeed possible to delay the injection one Earth-Jupiter synodic period by delaying the arrival date ~13 months in integer numbers of Callisto periods (Case D). Note the sinusoidal behavior of the delivered mass as the injection oscillates between favorable and unfavorable geometries.

Table 2 – Descriptions of the four trajectory scenarios illustrated in Figure 6

	Description
Case A	*Base Case*: Optimized for a 6-year flight time with free injection parameters and Jupiter arrival date. The injection C_3 (and corresponding initial mass) and Jupiter arrival date were fixed while the injection date was varied.
Case B	*Base Case with Modified Arrival Date:* Injection parameters fixed at the values for Case A, but the arrival date is delayed 5 Callisto Periods.
Case C	*Suboptimal 2.5 Rev Case:* Parameters are fixed at the values for Case A, but the arrival date is delayed 12 Callisto Periods (~7 mo.) and the trajectory family includes an additional half-revolution about the Sun.
Case D	*Base Case One Synodic Period Later*: Parameters are fixed at the values for Case A, but the trajectory (including arrival date) is shifted one synodic period later.

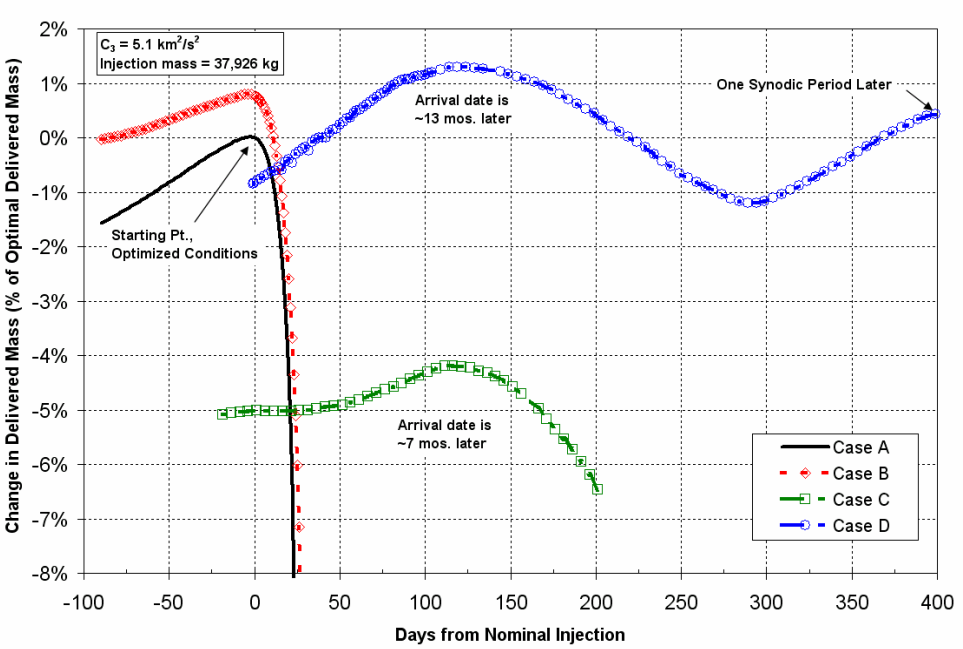

Figure 6 – Direct 6-year (Case 1) trajectory injection period results; multiple families considered

As with trajectory Case 1, Case 2 shows little performance improvement from a delayed arrival date within a particular trajectory family. This is illustrated by Case B in Figure 7. Each case in Figure 7 is described in detail in Table 3. Case B is the result of moving the arrival date for Case A approximately 6 months into the future, thereby increasing the flight time. Due to the geometry of the trajectory, however, there is very little benefit in this delay. However, when an alternate trajectory family is considered (in this case a 2-rev trajectory indicated by Case C in Figure 7) with an optimal injection date that occurs one year later, it is apparent that one could inject far in advance of the optimal injection date for that trajectory and be able to delay injection further than the previous family would allow with the same delay in arrival date. In the figure, this second trajectory family was constrained to have the same injection C_3 and corresponding initial mass as Case A to simulate an inability to change the spacecraft configuration after launching into the assembly orbit. Note again the sinusoidal behavior in the delivered mass as the injection geometry oscillates between favorable and unfavorable geometries.

Table 3 – Descriptions of the three trajectory scenarios illustrated in Figure 7

	Description
Case A	*Base Case*: 2.5 revolution trajectory optimized for a 7.5-year flight time with free injection parameters and Jupiter arrival date. Then the injection C_3 (and corresponding initial mass) and Jupiter arrival date were fixed while the injection date was varied.
Case B	*Base Case with Modified Arrival Date:* Parameters are fixed at the values for Case A, but the arrival date is delayed 12 Callisto Periods (~6 months).
Case C	*Suboptimal 2 Rev Case:* Parameters are fixed at the values for Case A, but the arrival date is delayed 11 Callisto Periods.

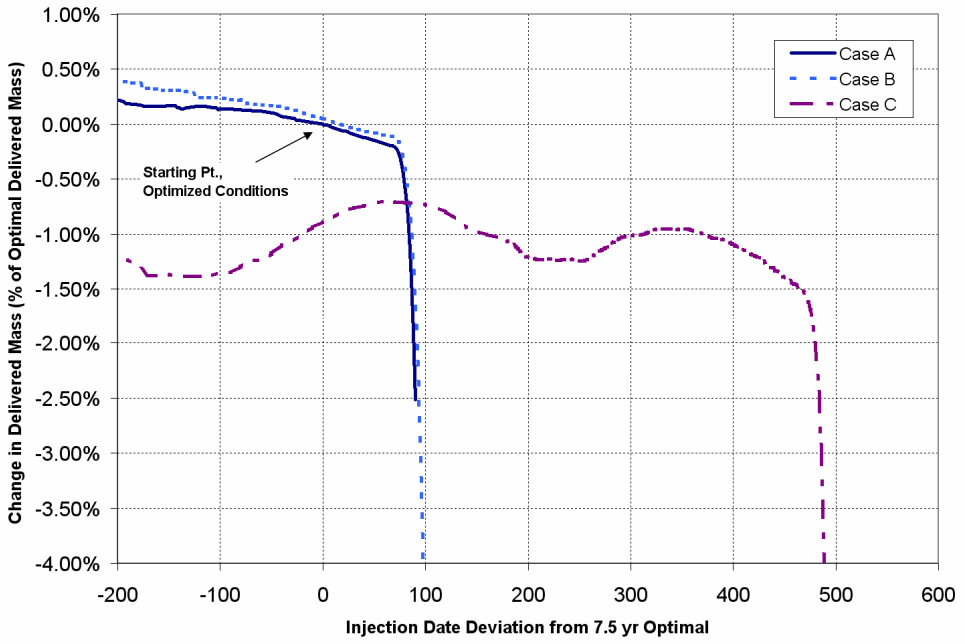

Figure 7 – Injection period for trajectory Case 2 and an alternate solution

The drop off in performance for Case C in Figure 7 occurs roughly one year after Cases A and B even though the arrival date was only delayed by half a year relative to the nominal (Case A). This is due to the change in trajectory family. Case C is a trajectory that performs roughly 2 heliocentric revolutions rather than 2.5 revolutions as in Cases A and B. This difference allows Case C to be a generally shorter trajectory at the cost of some delivered mass. The rest of the difference in delivered mass can be accounted for by the suboptimal C_3 and initial mass used for Case C to maintain consistency with the nominal case (Case A). An advanced mission study could be performed to determine an intermediate injection mass and C_3 that would provide nearly equivalent performance for both the 2-rev and 2.5-rev solutions.

In both the 6-year and 7.5-year trajectory examples (Figure 6 and Figure 7), allowing for different families of trajectory and arrival times offers the ability to extend the injection period indefinitely with minor impacts to delivered mass. By examining the alternative solutions that exist, one can trade changes in arrival date with injection period size and performance.

INJECTION VECTOR SENSITIVITY

Approach

The purpose of the injection-vector sensitivity study is two-fold. First of all, the study aims to characterize the trajectories' sensitivities to errors in the injection execution to allow sufficient margins in the mission design. Second, the injection direction perturbations feed directly into the injection opportunities analysis by defining the range of acceptable departure directions about the optimal. This is explained in greater detail in the next section.

In each of the injection vector sensitivity experiments, the departure and arrival dates and the injection mass were held fixed at the optimized values for each trajectory case. The arrival date is maintained to preserve the Jovian tour (as described in the Injection Period section). The injection date and mass are held fixed because it is not reasonable to be able to either predict the injection errors, and therefore optimize the injection date and mass around the errors, or to plan the assembly orbit's orientation in anticipation of exactly when during the injection period the spacecraft will inject. The latter would negate the need for an injection period. Hence, these assumptions are consistent with the study objectives stated above.

The first injection-vector sensitivity experiment explores the effects of introducing deviations in the injection C_3 magnitude. In order to isolate the impact of magnitude versus direction variations, the injection direction is held constant while the magnitude is incrementally increased or decreased from the optimal value. The thrust profile is re-optimized at each step to yield the greatest mass at Jupiter arrival. It is reasonable to assume that the thrust profile could be re-designed in such an event because each trajectory requires coasting for the first 60 days after injection.

The second experiment in this study is the reverse of the first: the injection C_3 is held constant while the direction is modified. Both the right ascension of the injection asymptote (RLA) and the declination of the injection asymptote (DLA) are parametrically varied. (Although we distinguish between launch and injection, we use the conventional terms of RLA and DLA to describe the Earth departure asymptote.) This experiment serves to characterize the sensitivity to small errors in the injection execution as well as to define the acceptable RLA and DLA ranges used in calculating the injection opportunities.

Injection C_3 Variation Results

The mass-performance impacts of varying the injection C_3 by ±10% for trajectory Cases 1 and 3 and ±20% for Cases 2 and 4 are shown in Figure 8. Each case has its own reference value for the C_3 (see Table 1), however, so a 20% change in Case 4 (2 km^2/s^2), for example, is very different from the same percent change in Case 2 (0.07 km^2/s^2). The horizontal axis shows the percent change from the optimal C_3, and the vertical axis gives the percent change in the final mass (mass at Jupiter arrival) relative to the optimal mass.

In Case 1, the performance impact of an injection under-burn is more significant than with any other trajectory. Case 1 suffers from having only one optimal coast period (Figure 2), so there are limited opportunities to apply additional thrusting to compensate for an underperforming injection burn. The worst instance shown, however, is less than a 1.7% mass decrease for a rather substantial under-burn of 10% of the C_3. An over-burn, on the other hand, means less ΔV must be applied by the electric propulsion system to achieve the Jupiter arrival date. An increase in the C_3 therefore yields a higher final mass, as shown in Figure 8.

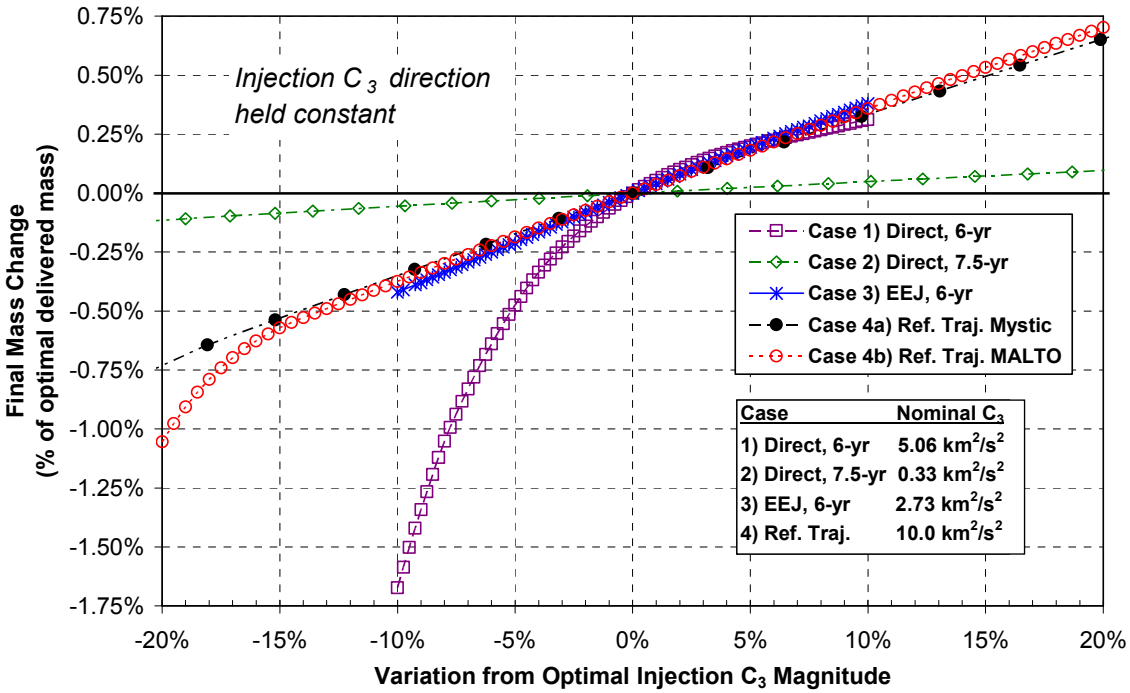

Figure 8 – Mass Impact of Varying the Injection C_3 Magnitude

Case 2, on the other hand, is relatively insensitive to proportionally sizeable changes in the injection C_3. This is due in a large part to the optimal injection C_3 of only 0.33 km^2/s^2, which is an order of magnitude lower than for the other cases. A 20% change in the C_3 is a delta of only 0.07 km^2/s^2, so a 20% under-burn would not burden the NEP system with much additional ΔV. Although not shown in Figure 8, C_3 variations of up to ±50% were computed, but the relative mass changes only ranged from -0.32% to +0.23%. This trajectory also benefits from two optimal coasting periods during its 7.5-year flight time (Figure 2), so there are ample opportunities to make up for any energy lost from the reduced injection C_3.

Because it is the only trajectory with a gravity assist, Case 3 has a unique set of constraints compared to the other cases. Not only does the spacecraft have to rendezvous with Jupiter on a fixed date, it must also target an Earth flyby to get to Jupiter. Despite this added complexity, Case 3 handles ±10% C_3 magnitude variations better than Case 1. Even if one considers the actual value of injection energy change, a loss of 0.25 km^2/s^2 results in a shortfall of 0.47% mass in Case 1 but only 0.39% in Case 3. Figure 2 also shows that Case 3 has several optimal coast arcs where additional thrusting can be applied, which tends to reduce the sensitivity to injection magnitude errors.

The plots of both Cases 4a and 4b in Figure 8 are especially interesting because of how the results from these cases compare to one another. From +20% down to nearly -15% of the optimal C_3, the results from Mystic and MALTO are nearly indistinguishable. In fact, if the C_3 is increased by as much as 50% (not shown in Figure 8), the Case 4b results are still in extremely close agreement with the Case 4a values. This discovery is significant because it validates the use of MALTO, a lower-fidelity preliminary-design tool, for analyzing the effects of injection perturbations. At C_3 magnitude deviations beyond -15%, MALTO provides a more conservative estimate than Mystic, but there is only a 0.3% mass difference between them at a 20% decrease in the injection C_3.

Overall, the NEP system could produce trajectories that are fairly insensitive to errors in the C_3 magnitude. In all cases studied, an over-burn means that less low-thrust ΔV is required, so less propellant is expended on the interplanetary trajectory. As for instances of an under-burn, even the most sensitive

case, Case 1, can tolerate a 5% reduction in the C_3 and still only have the mass at Jupiter diminished by 0.5%. The same mass reduction limit of 0.5% can be maintained on Case 4, the Reference Trajectory, with an injection underperformance of 15%!

Injection Asymptote Variation Results

Having shown that using nuclear-electric propulsion can result in a low sensitivity to injection magnitude errors, we now turn to the question of how a NEP trajectory is impacted by deviations in the injection asymptote. The optimal injection directions, RLA and DLA,[**] are given in Table 4. The differences in the optimal RLA and DLA for Cases 4a and 4b are attributed to their different injection dates. The geometry of the injection is tied to the Earth's location at the injection epoch, and Case 4b injects about 15 days later than Case 4a (see Table 1). Since the Earth moves roughly 1º/day in its orbit, the 15º RLA difference between Cases 4a and 4b is expected.

Table 4 – Optimal Injection Direction for Each Trajectory Case[**]

Case	Optimal RLA (deg)	Optimal DLA (deg)
1	122.8	20.5
2	182.8	1.6
3	234.7	-19.4
4a	170.2	5.7
4b	185.6	-0.9

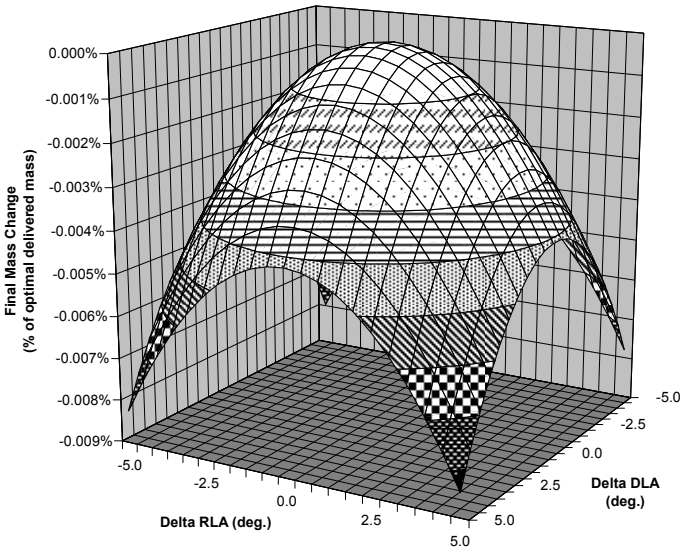

Figure 9 – Mass Impact of Varying the in Injection Direction on Trajectory Case 2

Figure 9 shows the mass impact of varying the RLA and DLA by ±5º on Case 2. The two horizontal axes give the amount of change from the optimal injection direction. The vertical axis represents the percent change in mass at Jupiter arrival relative to the mass when injecting in the optimal direction. Note that injecting 5º from the optimized values of both RLA and DLA results in a tiny mass change of less than

[**] Earth Equator and Equinox of J2000 inertial reference frame (EME2000)

3 kg, or 0.009%! As with the C_3 magnitude variations, Case 2 is quite impervious to changes in the injection V_∞ direction. This insensitivity is due to the very low C_3 (only 0.33 km^2/s^2), which means this trajectory does not depend heavily on the precise injection conditions. In addition, the relatively long flight time of 7.5 years means there is sufficient time to use the NEP engines to impart the required ΔV and therefore plenty of time to correct any changes to the planned injection conditions.

In Cases 1 and 3, we broadened the RLA range to ±20º to explore the possibility of intentionally injecting in an off-nominal direction. It is possible that the node of the assembly orbit will not align with the optimal injection asymptote at the instant injection is desired. Rather than relying on the injection vehicle to perform a costly plane change to reach the optimal departure asymptote, we investigate the performance impact of using the NEP system to compensate for the sub-optimal injection direction.

Figure 10 shows the results of injection direction variations of ±20º and ±5º in RLA and DLA, respectively, for Case 1. Case 1 exhibits a much greater sensitivity to injection asymptote deviations than Case 2. Even if the RLA range is constrained to ±5º, the mass loss is as high as 0.13% (versus 0.009% for Case 2). Also note the "cliff" in performance when the RLA deviation exceeds +15º. While injecting with an RLA value less than the optimal (negative delta-RLA) causes the NEP system to compensate for the sub-optimal departure asymptote, injecting at higher RLA values leads to issues with orbital energy, as well. The RLA is measured in the counterclockwise direction, so increasing the departure RLA means that the injection asymptote is directed closer to the Sun. If the RLA is increased far enough, the injection burn will leave the spacecraft with notably less orbital energy with respect to the Sun than the optimal injection would provide. At that point, the NEP system must compensate for this energy deficiency, and the cost is nearly 3 km/s in low-thrust ΔV.

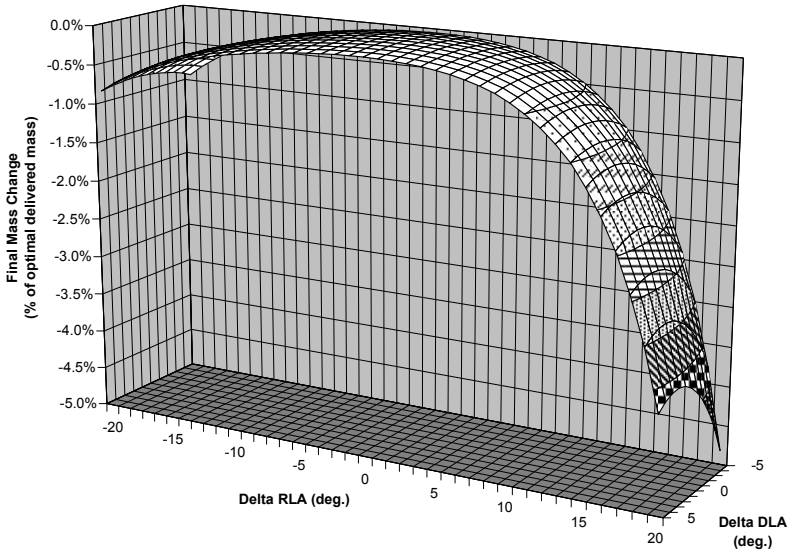

Figure 10 – Mass Impact of Varying the in Injection Direction on Trajectory Case 1

Despite these obstacles, Case 1 can abide a wide RLA range without unreasonable mass losses. A range of at least -20º to +13º in delta RLA (RLA deviations beyond -20º were not evaluated) and ±5º in delta DLA results in a mere 1% mass decrease. If only a 0.5% mass loss can be tolerated, the full extent of the DLA values and RLA values of -16º to +10º are available.

Trajectory Case 3, however, does not have a steep drop-off in performance when the same DLA and RLA ranges are computed (see Figure 11). It was expected that this trajectory would be more sensitive

to variations in the injection conditions than Case 1, which has the same total flight time, because it must target the intermediate flyby of Earth in addition to arriving at Jupiter on a fixed date. This is obviously not the case, however, and the full RLA and DLA ranges of ±20º and ±5º, respectively, result in mass losses of less than 0.5%. (Note that the "indentations" in the Figure 11 surface plot are due to the convergence tolerances used in performing this analysis.)

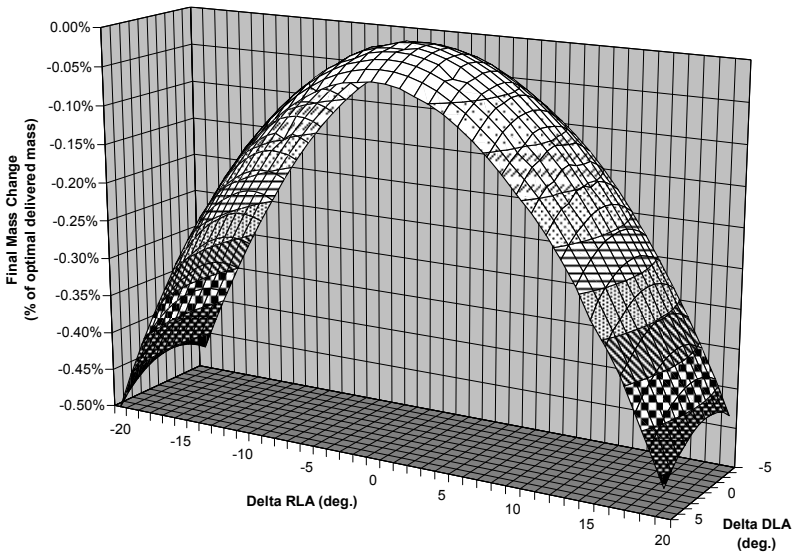

Figure 11 – Mass Impact of Varying the in Injection Direction on Trajectory Case 3

One reason Case 3 is less affected by injection asymptote changes is the greater number of optimal coast arcs in this trajectory compared with Case 1. Case 1 only has one optimal coast arc during which it can compensate for sub-optimal injection conditions. This coast arc also occurs a long time after injection (see Figure 2). If there were an optimal coast arc in Case 1 closer to injection, less ΔV would be required to maintain the Jupiter arrival date. Case 3, though, has several optimal coast arcs, many of which are early in the trajectory, as shown in Figure 2. Also, Case 3 has a lower optimal C_3 than Case 1 (see Table 1), so it can be thought of as a smaller vector going in the "wrong" direction, which suggests it should be easier to correct post-injection. This trajectory has more flexibility to cope with sub-optimal injections and therefore does not exhibit the "cliff" in performance that Case 1 has, shown in Figure 10.

The response to injection asymptote perturbations of Case 4b, the MALTO representation of the Reference Trajectory, is given in Figure 12. This figure shows a greater RLA range of ±25º, versus ±20º for Cases 1 and 3. Like Case 1 (Figure 10), there is a steep drop-off in performance at large increases in the RLA. However, the "cliff" for Case 4b does not manifest itself until the RLA is increased by approximately 22º, which is in a range not covered by the analyses of Cases 1 through 3. In the RLA variation range of ±20º, the largest mass loss for Case 4b is 0.5%, which puts this trajectory on par with Case 3 (shown in Figure 11).

A comparison of the results of varying the injection direction for Cases 4a and 4b is given in Figure 13 with both cases plotted against the same vertical scale. (Case 4a was computed at a finer mesh, so the grid lines in Figure 13 are more closely-spaced in the plot on the left.) The correspondence between the two plots is quite remarkable, especially the negative delta RLA values. It is only at the largest RLA increases that the Mystic and MALTO representations begin to differ significantly. At an RLA increase of 20º, the greatest mass loss in both cases occurs when the DLA is increased by 5º, and the disparity between the Case 4a and 4b mass changes at that point is only 0.05%.

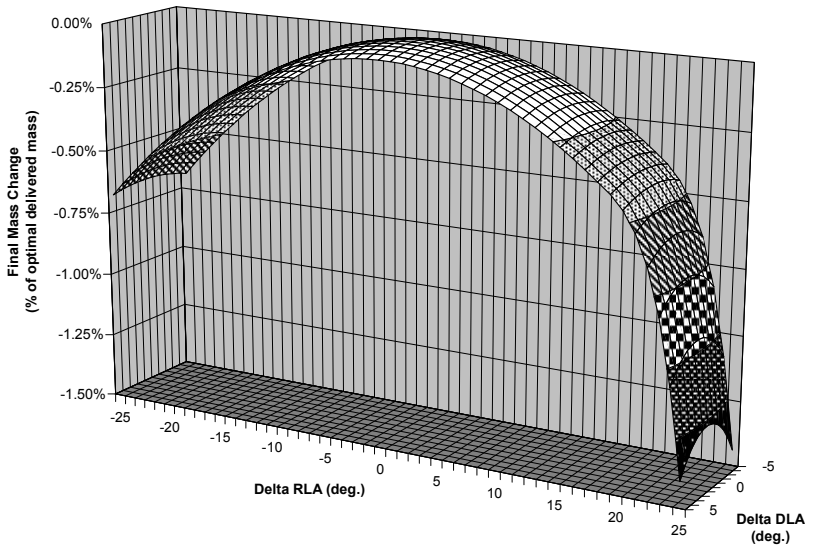

Figure 12 – Mass Impact of Varying the Injection Direction on Trajectory Case 4b

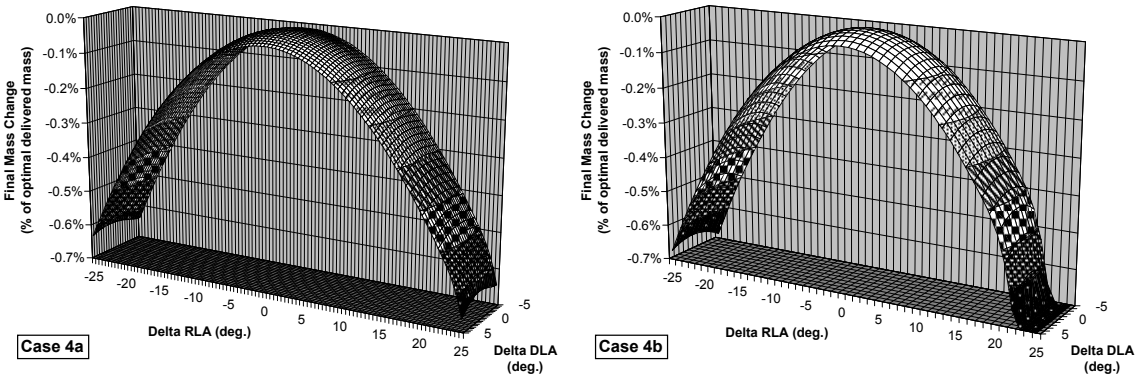

Figure 13 – Mass Impact of Varying the Injection Direction on Trajectory Cases 4a and 4b

When the differences in how Mystic and MALTO model trajectories are considered (i.e. level of fidelity, force models, etc.), the good agreement between their results, evident in Figure 13 as well as Figure 8, is an additional validation of the use of MALTO for performing injection V_∞ variation analyses. Furthermore, Figure 13 illustrates the low sensitivity of Case 4a to variations in the injection asymptote. For an extensive RLA range of ±25º and a DLA range of ±5º, the mass hit is less than 0.7%. Using the NEP system for this mission can enable a wide range of injection directions without substantial mass performance impacts.

INJECTION OPPORTUNITIES

Approach

For a launch from the surface of the Earth to an interplanetary departure trajectory, the primary problem is to match the required V_∞ vector to the specified site location.[16] In the mission architecture analyzed in this paper, however, the V_∞ vector must lie within the plane of a regressing assembly orbit for an

injection to be possible. Furthermore, the spacecraft must be phased within the assembly orbit such that the final burn of the final stage takes place at the perigee of the interplanetary hyperbolic trajectory.

Unlike the case of launching from the surface of the Earth, for which in general two injection solutions exist per day, an assembly orbit that is properly located for injection on one day may be incorrectly phased on the following day. The RAAN of an assembly orbit at 400 km altitude and at an inclination of 28.5º regresses at a rate of 7.1º/day. For typical values and rates of change of DLA and RLA of interplanetary trajectories, such an assembly orbit will quickly regress away from the desired targets and another opportunity will not be available until the orbit has regressed 180º. As a consequence, there may be many days within the injection period in which injection from the assembly orbit is not possible.

To increase the number of injection opportunities during the injection period, a targeting tolerance is placed on the nominal RLA and DLA. By allowing the spacecraft to inject into a range of departure asymptotes that are close to the optimal, the number of days when injection is possible is greatly increased. The number of injection opportunities per day and the duration of the injection window are also increased.

Results

A representative assembly orbit, with an altitude of 400 km, an inclination of 28.5º, and a RAAN chosen to place the first injection opportunity near the beginning of the injection period, was propagated for the duration of the 84-day injection period given in Figure 14. Each orbit rev during that time was checked to determine if the optimal departure asymptote or any of the nearby asymptotes lay within the orbit plane. If the orbit was aligned correctly and the spacecraft properly phased to allow for an injection burn at the correct position and time, an injection opportunity was defined to exist. The injection period in Figure 14 is taken from the injection period analysis of trajectory Case 4a (also shown in Figure 4). The optimal RLA and DLA targets for that case are given in Figure 15.

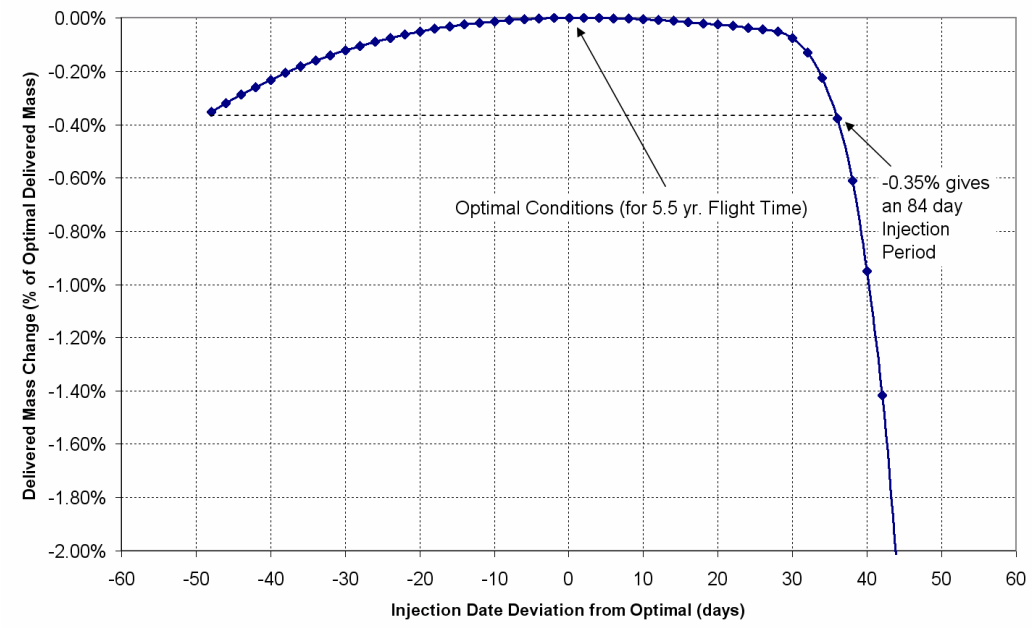

Figure 14 – Reference injection period (Case 4a)

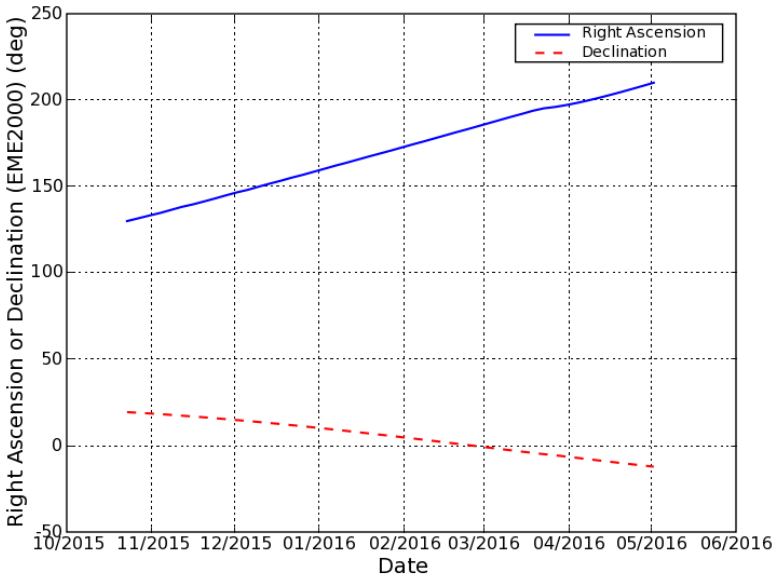

Figure 15 – Optimized RLA & DLA targets[**]

The injection opportunities fall into "clusters" that represent the times when the plane of the orbit is near the group of departure asymptotes that are considered acceptable. These clusters are further broken down into ascending opportunities, corresponding to the ascending side of the assembly orbit, and the descending opportunities, corresponding to the descending side of the assembly orbit. The maximum number of injection opportunities per day is equal to the number of orbit revs per day. In this case, the orbital period is 1.54 hours, so the maximum number of injection opportunities in a given day is either 15 or 16. Figure 16 shows an example case in which injections to asymptotes with a DLA within ±2º of the nominal value and an RLA within ±25º of the nominal value are allowed.

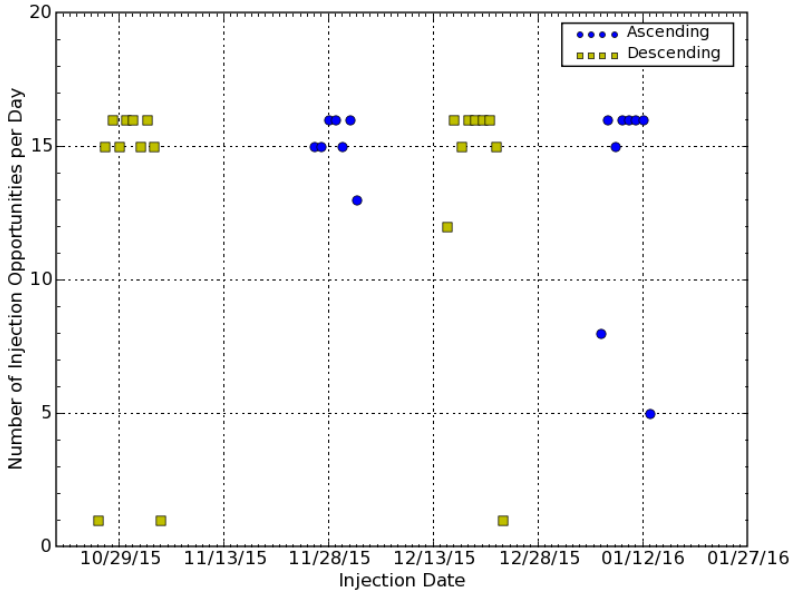

Figure 16 – Targeting tolerance and injection opportunities (±25° in RLA; ±2° in DLA)

For injection onto the nominal departure asymptote, the final stage burn must take place at an instantaneous point in time. If a targeting tolerance is allowed, however, the final stage burn may take place during a finite injection window, analogous to a conventional launch window. Figure 17 shows the duration of the injection window as a function of the RLA and DLA targeting tolerances.

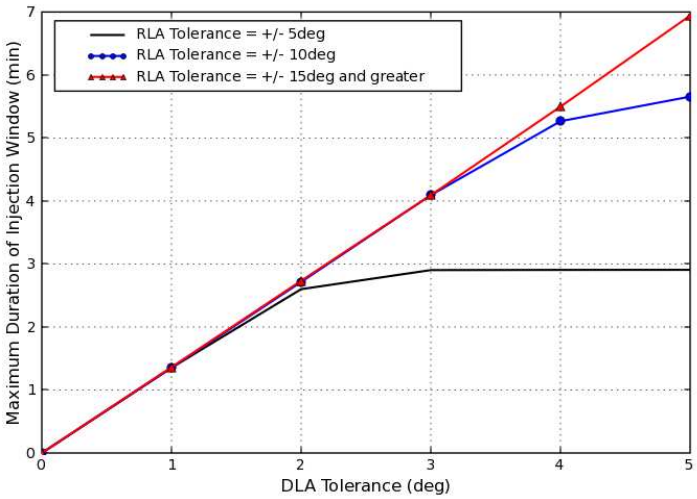

Figure 17 – Injection Opportunity Window and Targeting Tolerance

Figure 18 shows the effects of RLA and DLA targeting tolerances for the assembly orbit described earlier. Moderate targeting allowances, e.g. ±10º in RLA and ±3º in DLA, allow for injection on 20 days out of the 84-day injection period, which is comparable to the launch period of a typical interplanetary mission launched from the surface of the Earth. However, the total number of injection opportunities is much greater because many of those days may support the maximum of 15 or 16 injection opportunities per day.

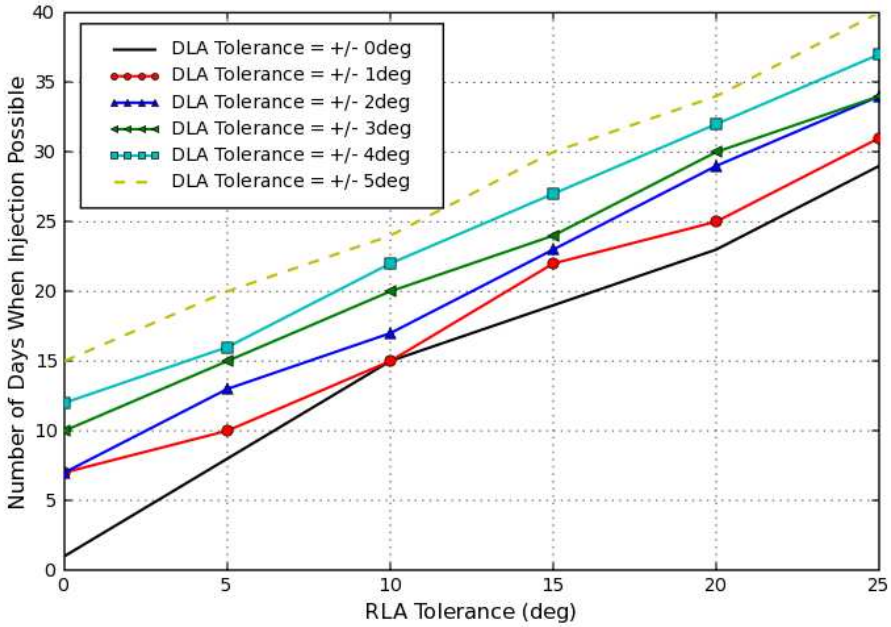

Figure 18 – Total Number of Injection Opportunities

Targeting tolerances of ±25º in RLA and ±5º in DLA, which increase the number of possible injection days to 40, can be sustained without a substantial impact on the delivered mass, as shown in Figure 13, but this assumes a perfect injection by the final stage of the injection vehicle. Injection dispersions must be considered when determining tolerances on the RLA and DLA, but even modest tolerances greatly increase the number of days and opportunities for injection and thus the probability of injection.

CONCLUSIONS

Nuclear-electric propulsion trajectories to Jupiter can allow for a substantial injection period, broad RLA ranges, and multiple Earth-departure opportunities over the injection period without great sacrifices in mass performance. Using the NEP system and allowing for different trajectory families and arrival times can offer the ability to extend the injection period indefinitely with minor impacts to delivered mass. By examining alternative solutions, one can trade changes in arrival date with injection period length and performance. In addition, employing a NEP system could yield trajectories that are rather insensitive to errors in the injection V_∞ vector as well as planned variations in the injection direction.

Trajectories that had lower optimal injection C_3 values, longer flight times, and/or longer and more numerous coast arcs were less sensitive to injection vector variations and injection date. Lower C_3 solutions reduced the sensitivity of the injection period and the injection vector due to the diminished impact of unfavorable geometry. The longer flight times and increased coasting durations allowed higher C_3 cases to compensate for sub-optimal injection conditions. The large RLA range provided by the NEP system, coupled with long injection periods, increases the probability of achieving Earth departure and fulfilling the mission requirements.

ACKNOWLEDGEMENTS

The authors would like to thank Jon Sims and Louis D'Amario for their guidance and leadership in directing the work presented in this paper. We are also grateful Paul Finlayson, Edward Rinderle, Gregory Whiffen, and Benjamin Engebreth for their work developing and enhancing the low-thrust trajectory optimization software used in these analyses. This work was performed at the Jet Propulsion Laboratory, California Institute of Technology, under a contract with the National Aeronautics and Space Administration.

REFERENCES

1. Williams, S. N., and Coverstone-Carroll, V., "Benefits of Solar Electric Propulsion for the Next Generation of Planetary Exploration Missions," *Journal of the Astronautical Sciences*, Vol. 45, No. 2, April-June 1997, pp. 143-159.

2. Sauer, C. G., Jr., and Yen, C. L., "Planetary Mission Capability of Small Low Power Solar Electric Propulsion Systems," IAA-L-0706, IAA International Conference on Low-Cost Planetary Missions, Laurel, MD, April 12-15, 1994.

3. Rayman, M. D., and Lehman, D. H. "NASA's First New Millennium Deep-Space Technology Validation Flight," IAA-L-0502, Second IAA International Conference on Low-Cost Planetary Missions, Laurel, MD, April 16-19, 1996.

4. Betts, J. T., "Optimal Interplanetary Orbit Transfers by Direct Transcription," *Journal of the Astronautical Sciences*, Vol. 42, No. 3, 1994, pp. 247-268.

5. Kluever, C. A., "Optimal Low-Thrust Interplanetary Trajectories by Direct Method Techniques," *Journal of the Astronautical Sciences*, Vol. 45, No. 3, 1997, pp. 247-262.

6. McConaghy, T. T., Debban, T. J., Petropoulos, A. E., and Longuski, J. M., "Design and Optimization of Low-Thrust Trajectories with Gravity Assists," *Journal of Spacecraft and Rockets*, Vol. 40, No. 3, May-June, 2003, pp. 380-387.

7. Debban, T. J., McConaghy, T. T., and Longuski, J. M., "Design and Optimization of Low-Thrust Gravity-Assist Trajectories to Selected Planets," AIAA/AAS Astrodynamics Specialists Conference, AIAA Paper 2002-4729, Monterey, CA, August 5-8, 2002.

8. Maddock, R. W., and Sims, J. A., "Trajectory Options for Ice and Fire Preproject Missions Utilizing Solar Electric Propulsion," AIAA/AAS Astrodynamics Specialists Conference, AIAA Paper 98-4285, Boston, MA, August 10-12, 1998.

9. Yam, C. H., McConaghy, T. T., Chen, K. J., and Longuski, J. M., "Preliminary Design of Nuclear Electric Propulsion Missions to the Outer Planets," AIAA/AAS Astrodynamics Specialist Conference, AIAA Paper 2004-5393, Providence, RI, August 16-19, 2004.

10. Parcher, D. W., and Sims, J. A., "Venus and Mars Gravity-Assist Trajectories to Jupiter Using Nuclear Electric Propulsion," AAS/AIAA Astrodynamics Specialists Conference, AAS Paper 05-112, Copper Mountain, CO, January 23-27, 2005.

11. Parcher, D. W., and Sims, J. A., "Earth Gravity-Assist Trajectories to Jupiter Using Nuclear Electric Propulsion," AAS/AIAA Astrodynamics Specialists Conference, AAS Paper 05-397, Lake Tahoe, NV, August 7-11, 2005.

12. Parcher, D. W., and Sims, J. A., "Gravity-Assist Trajectories to Jupiter Using Nuclear Electric Propulsion," AAS/AIAA Astrodynamics Specialists Conference, AAS Paper 05-398, Lake Tahoe, NV, August 7-11, 2005.

13. Sims, J. A., and Flanagan, S. N., "Preliminary Design of Low-Thrust Interplanetary Missions," AAS/AIAA Astrodynamics Specialists Conference, AAS Paper 99-338, Girdwood, AK, August 16-19, 1999.

14. Whiffen, G. A., and Sims, J. A., "Application of Novel Optimal Control Algorithm to Low-Thrust Trajectory Optimization," AAS/AIAA Space Flight Mechanics Conference, AAS Paper 01-209, Santa Barbara, CA, February 11-15, 2001.

15. Whiffen, G. A., Lam, T., Kangas, J. A., and Russell, R. P., "The Jupiter Icy Moons Orbiter Reference Trajectory," AAS/AIAA Space Flight Mechanics Conference, AAS Paper 06-[xxx], Tampa, FL, January 22-26, 2006.

16. Sergeyevsky, Andrey B., Gerald C. Snyder, Ross A. Cunniff, "Interplanetary Mission Design Handbook, Volume 1, Part 2," JPL Publication 82-43, September 15, 1983.